

Journal Pre-proof

Enhanced red emission from Bi³⁺ sensitized CaWO₄:Eu³⁺ as red component for near UV/blue LED pumped white light emission

Takhe Yaba, Ranjoy Wangkhem, N. Shanta Singh



PII: S0925-8388(20)32386-0

DOI: <https://doi.org/10.1016/j.jallcom.2020.156022>

Reference: JALCOM 156022

To appear in: *Journal of Alloys and Compounds*

Received Date: 5 May 2020

Revised Date: 29 May 2020

Accepted Date: 9 June 2020

Please cite this article as: T. Yaba, R. Wangkhem, N.S. Singh, Enhanced red emission from Bi³⁺ sensitized CaWO₄:Eu³⁺ as red component for near UV/blue LED pumped white light emission, *Journal of Alloys and Compounds* (2020), doi: <https://doi.org/10.1016/j.jallcom.2020.156022>.

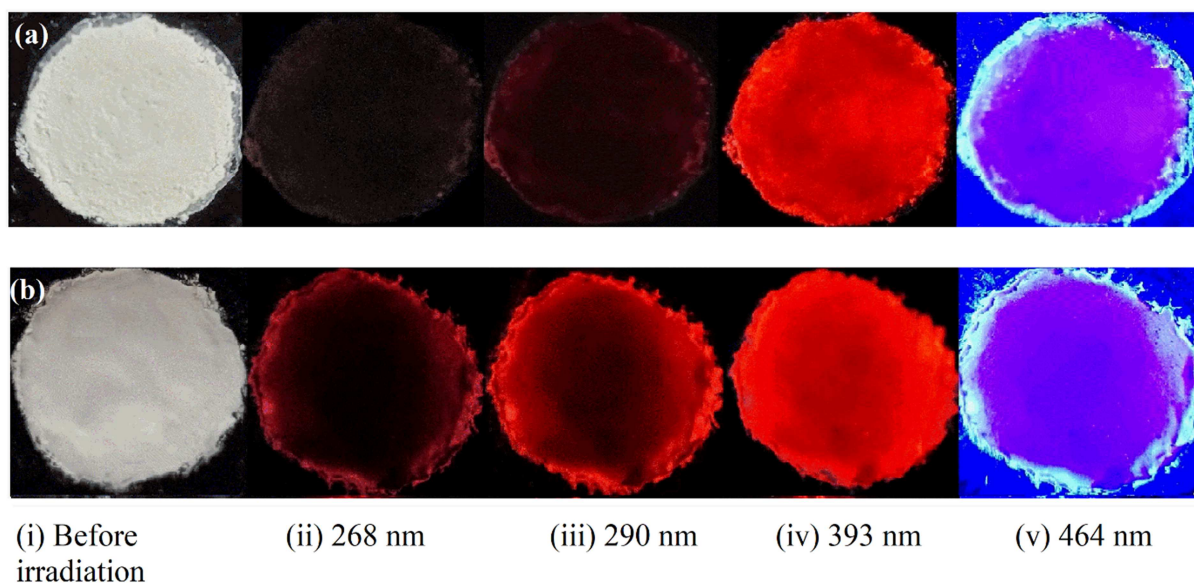
This is a PDF file of an article that has undergone enhancements after acceptance, such as the addition of a cover page and metadata, and formatting for readability, but it is not yet the definitive version of record. This version will undergo additional copyediting, typesetting and review before it is published in its final form, but we are providing this version to give early visibility of the article. Please note that, during the production process, errors may be discovered which could affect the content, and all legal disclaimers that apply to the journal pertain.

© 2020 Published by Elsevier B.V.

CRedit authorship contribution statement

Takhe Yaba: Writing – Original Draft, Investigation, Formal analysis. **Ranjoy Wangkhem:** Writing – Review & Editing. **Naorem Shanta Singh:** Supervision, Writing – Original Draft, Writing – Review & Editing.

Journal Pre-proof



Photographs of (a) as prepared $\text{CaWO}_4:\text{Eu}^{3+}(5 \text{ at.}\%)/\text{Bi}^{3+}(11 \text{ at.}\%)$ and (b) $500 \text{ }^\circ\text{C}$ annealed $\text{CaWO}_4:\text{Eu}^{3+}(5 \text{ at.}\%)/\text{Bi}^{3+}(5 \text{ at.}\%)$ sample under the exposure of (i) 268 nm, (ii) 290 nm, (iv) 393 nm and (v) 464 nm wavelength light sources.

Enhanced red emission from Bi³⁺ sensitized CaWO₄:Eu³⁺ as red component for near UV/blue LED pumped white light emission

Takhe Yaba, Ranjoy Wangkhem and N. Shanta Singh*

Department of Physics, Nagaland University, Lumami-798627, Nagaland, India

Abstract

Bi³⁺ (y = 0 – 15 at.%) sensitized CaWO₄:Eu³⁺ (5 at.%) red emitting phosphors were successfully prepared by hydrothermal method. All the samples generated intense red emission under the excitation at 393 and 464 nm. The incorporation of Bi³⁺ in CaWO₄ does not induce any interference among the optical properties of WO₄²⁻ and Bi³⁺. The sensitization with Bi³⁺ in CaWO₄:Eu³⁺ leads to the enhancement of ~393 nm (⁷F₀ → ⁵L₆) and ~464 nm (⁷F₀ → ⁵D₂) absorption peak of Eu³⁺. At optimal concentration of Bi³⁺, the enhancement is 5 and 10 for ~393 nm (⁷F₀ → ⁵L₆) and ~464 nm (⁷F₀ → ⁵D₂), respectively. A further enhancement in emission at optimized Bi³⁺ concentration by a factor of ~5.8 and ~22 under the respective excitation of 393 and 464 nm is observed after annealing the samples at 500 °C. The energy transfer efficiency from Bi³⁺ to Eu³⁺ was improved from 75% to 95% post annealing. The energy transfer process is observed to be occurred mainly due to dipole-dipole interactions. The CIE chromaticity coordinates reveal the nearly 100% saturation of red color emission.

Keywords: Photoluminescence; energy transfer; red emitting phosphor; n-UV/blue light

*Corresponding author

E-mail: ssaorem@nagalanduniversity.ac.in (N.S. Singh), +91-9862032690

1. Introduction

Lately, white light emitting diodes (w-LEDs) have attracted much interest in lighting industries due to their significant long working lifetime, higher efficiency, low energy consumption, eco-friendly and less thermal radiations [1-8]. White LEDs, therefore, have the advantage over widely used incandescent and fluorescent lamps [9-11]. Mostly, w-LEDs are achieved by a combination of LED chip with down-converting phosphors and they are known as phosphor converted white LEDs (pc-LEDs). The commercially available w-LEDs are produced by a combination of yellow phosphor (e. g. $\text{Y}_2\text{Al}_2\text{O}_{12}:\text{Ce}^{3+}$) with InGaN blue LED chip working in the wavelength range of 450–470 nm [12-16]. However, this approach has some drawbacks in the quest of (i) high color rendering index (CRI > 90), (ii) lower correlated color temperature (2700–4000 K) primarily due to the lack of efficient red emitting component [17-20]. The alternative ways to generate white light with better CRI are (i) by coating a near UV (n-UV) LED chip with a mixture of blue, green and red emitting phosphors and (ii) blue LED chip combined with green and red phosphor [21,22]. In these approaches, an efficient red phosphor is required. Therefore, the demand for potential and stable red emitting phosphor, which can be efficiently excited either by n-UV or blue light, dramatically increases. In this aspect, recent reports are available on red emitting phosphors activated with Eu^{2+} or Eu^{3+} . Generally, these red phosphors include thermally stable nitride/oxynitride/garnet phosphors activated with Eu^{2+} , e.g. $\text{Sr}_2\text{Si}_5\text{N}_8:\text{Eu}^{2+}$ [23], $\text{Sr}[\text{LiAl}_3\text{N}_4]:\text{Eu}^{2+}$ [24], $\text{M}_2\text{Si}_5\text{N}_8:\text{Eu}^{2+}$ (M = Eu, Sr, Ba) [25], $\text{Sr}_3\text{Y}_2\text{Ge}_3\text{O}_{12}:\text{Eu}^{2+}$ [26], etc. They have shown promising broad absorption in ~400–480 nm which is well matched with the blue emission from InGaN based LEDs. However, their emission band is very broad, extending beyond human eye sensitivity limit (~700 nm) and, hence, they have lower luminescence efficacy [27]. Moreover, such phosphors require the synthesis conditions of reduced atmosphere and high temperature leading to higher investment. On the other hand, the very efficient Eu^{3+} activated phosphors with high color saturation such as $\text{Gd}/\text{YVO}_4:\text{Eu}^{3+}$ [28,29], $\text{Gd}_2\text{ZnTiO}_6:\text{Eu}^{3+}$ [30], $\text{CaMoO}_4:\text{Eu}^{3+}$ [31], $\text{CaWO}_4:\text{Eu}^{3+}$ [32,33], etc. are normally excited through the charge/energy transfer from the host matrix excited in the UV region. This limits their use as red component in w-LEDs with n-UV/blue LED chips as a pumping source.

However, Eu^{3+} emission has gain interest lately thanks to the new ways: (i) enhancement of $f-f$ absorptions of Eu^{3+} mainly ~394 nm (${}^7\text{F}_0 \rightarrow {}^5\text{L}_6$) and ~464 nm (${}^7\text{F}_0 \rightarrow {}^5\text{D}_2$) through sensitization, (ii) developing new type of composite host matrix etc. which are suitable for n-UV/blue LED chip excitation. With regard to later means, Du and Yu reported

the shift in the charge transfer band at 379 nm with enhanced absorption when the tungstate and molybdate are formed as a composite viz., $\text{La}_2\text{MoO}_6\text{-La}_2\text{WO}_6$ structure activated with Eu^{3+} [34]. We have also recently reported the enhanced ~ 393 nm (${}^7\text{F}_0 \rightarrow {}^5\text{L}_6$) and ~ 464 nm (${}^7\text{F}_0 \rightarrow {}^5\text{D}_2$) absorption peaks of Eu^{3+} in Bi^{3+} sensitized $\text{CaMoO}_4\text{:Eu}^{3+}$ red nanophosphor which possibly is suitable for n-UV/blue LED pumped w-LEDs [35]. One such promising candidate is $\text{CaWO}_4\text{:Eu}^{3+}$ which has excellent thermal and chemical stability and good optical properties [32,33,36]. In this front, P. Du *et al.* recently reported the enhancement of ~ 464 nm (${}^7\text{F}_0 \rightarrow {}^5\text{D}_2$) absorption peak of Eu^{3+} in Bi^{3+} sensitized $\text{CaWO}_4\text{:Eu}^{3+}$ which can be suitable for blue LED pumped red emission [37]. There are also reports on the enhanced energy transfer from the Bi^{3+} (sensitizer) to the Eu^{3+} (activator) ions in $\text{CaWO}_4\text{:Eu}^{3+}$ [38,39]. Xia *et al.*, reported the enhanced luminescence excited by ~ 392 nm (${}^7\text{F}_0 \rightarrow {}^5\text{L}_6$) due to lower crystal symmetry in Mg^{2+} and Sr^{2+} co-doped $\text{CaWO}_4\text{:Eu}^{3+}$ phosphor [40].

In this study, we report on hydrothermally synthesized $\text{Bi}^{3+}/\text{Eu}^{3+}$ co-doped CaWO_4 nanophosphor and the influence of Bi^{3+} sensitization. The effect of Bi^{3+} sensitization and annealing on the optical properties of $\text{CaWO}_4\text{:Eu}^{3+}$ is thoroughly discussed. We also report the mechanism of the energy transfer from sensitizer to activator in $\text{CaWO}_4\text{:Eu}^{3+}$ nanocrystals. The details of photoluminescence (PL), PL decay lifetime, quantum yield and coordinates in Commission Internationale de l'Éclairage (CIE) chromaticity diagram are discussed.

2. Materials and methods

2.1 Sample preparation

All the syntheses were done via hydrothermal method. The raw materials calcium nitrate tetra hydrate ($\text{Ca}(\text{NO}_3)_2 \cdot 4\text{H}_2\text{O}$, $\geq 99\%$), sodium tungstate dihydrate ($\text{Na}_2\text{WO}_4 \cdot 2\text{H}_2\text{O}$, $\geq 99\%$), europium nitrate hexahydrate ($\text{Eu}(\text{NO}_3)_3 \cdot 6\text{H}_2\text{O}$, 99.9%), bismuth nitrate pentahydrate ($\text{Bi}(\text{NO}_3)_3 \cdot 5\text{H}_2\text{O}$, $\geq 98\%$), poly(acrylic)acid (PAA) and sodium hydroxide (NaOH , $\geq 97\%$) were purchased from Sigma-Aldrich and used without further purification. PAA was used as a capping agent. Typically, to synthesize Bi^{3+} (1 at.%) sensitized Eu^{3+} (5 at.%) activated CaWO_4 nanocrystals, 250 mg of $\text{Ca}(\text{NO}_3)_2 \cdot 4\text{H}_2\text{O}$, 19 mg of $\text{Eu}(\text{NO}_3)_3 \cdot 6\text{H}_2\text{O}$, and 20 mg of PAA were dissolved in 20 mL of de-ionized (DI) water under continuous stirring. Then 5.5 mg of $\text{Bi}(\text{NO}_3)_3 \cdot 5\text{H}_2\text{O}$ already dispersed in 5 mL of DI water was added to this solution. As a next step, 372 mg of $\text{Na}_2\text{WO}_4 \cdot 2\text{H}_2\text{O}$ was added and stirred well until a homogeneous solution

was formed. The pH of the solution was maintained at ~7 by addition of NaOH (1 M) solution. The obtained solution was then transferred into a 100 mL Teflon lined stainless steel autoclave and heated in an oven at 180 °C for 3 h. The precipitate so formed was separated with centrifugation and washed with deionized water and ethanol five times. The obtained precipitate was dried in the oven at 60 °C and grounded. All other samples were synthesized following the same procedure. The as-prepared samples were heated in a furnace at 500 °C for 3 h in the air.

2.2 Characterization

The phase purity and structural analysis of the samples were performed by using a Bruker, D8 Advance X-ray diffractometer with a Cu K_{α} ($\lambda = 1.5406$ Å). The Fourier transform infrared (FT-IR) spectroscopy studies were carried out using a Shimadzu (model 8400S) spectrometer. The transmission electron microscopy (TEM) and the high-resolution transmission electron microscopy (HR-TEM) images of the samples were recorded using an JEOL 2000FX. All the steady state luminescence spectra and decay lifetime measurements were carried out using a Horiba FluoroMax-4CP Spectrofluorometer equipped with 150 W xenon lamp and 25 W μ sec flash lamp as excitation light sources. For quantum yield measurement, a K-sphere ‘petite’ integrating sphere (Reflectivity: 94-97% (380 – 500 nm), 96-98% (500 – 1500 nm) (Photon Technology International (PTI)) was used. Before measurement, the instrument was calibrated with standard Rhodamine B dissolved in water (standard QY ~31%) with observed quantum yield (29±2%). All the measurements were performed at room temperature.

3. Results and Discussion

3.1 X-ray diffraction (XRD), FT-IR and TEM studies

The XRD patterns of (a) as-prepared and (b) 500 °C annealed Bi³⁺ ($y = 0, 5, 7$ and 9 at.%) sensitized 5 at.% Eu³⁺ codoped CaWO₄ (thereafter termed as CaWO₄:Eu³⁺ (5 at.)/Bi³⁺ (y at.)) nanocrystals are respectively displayed in Fig. S1 of the supplementary material. In all the patterns, the presence of tetragonal phase of CaWO₄ (ICDD card no. 41-1431) crystal system with scheelite structure having space group I41/a is observed [32,33]. It can be ascertained that the substitution of Eu³⁺ and Bi³⁺ ions occurs Ca²⁺ sites. This is due to the nearly equivalent ionic radii of Eu³⁺ ($r = 1.07$ Å), Bi³⁺ ($r = 1.17$ Å) and Ca²⁺ ($r = 1.12$ Å) for the coordination number of CN = 8. However, the substitution in the W⁶⁺ ($r = 0.41$ Å) lattice

site may be ignored due to large difference in ionic radii as well as larger charge difference. Therefore, in case of as prepared samples, co-doping of Bi^{3+} (~up to 9 at.%) and Eu^{3+} (5 at.%) ions do not induce (i) any deviation from the tetragonal phase of CaWO_4 crystal structure and (ii) formation of any other possible phases such as Bi_2O_3 , Eu_2O_3 etc. Thus, as-prepared samples has solid solution formation up to 9 at.% of Bi^{3+} . Earlier, we reported the limit of 9 at.% of Bi^{3+} for the solid solution formation in $\text{CaMoO}_4:\text{Eu}^{3+}$ [35]. However, $\text{CaWO}_4:\text{Eu}^{3+}$, after annealing at 500 °C, such limit is found to be ≥ 7 at.% of Bi^{3+} . This is confirmed from the observance of Bi_2O_3 peak in $\text{CaWO}_4:\text{Eu}^{3+}$ (5 at.%)/ Bi^{3+} (9 at.%) (indicated by the symbol ‘●’) of the Fig. S1b (ICDD card no. 01-074-1375) [41]. The average crystallite sizes (d) are calculated using Scherrer equation, [42]

$$d = k\lambda/\beta\cos\theta \quad (1)$$

where d is the average crystallite size, $k = 0.9$ is the Scherrer constant, $\lambda = 1.5406$ Å is the X-ray wavelength, β is the full width half maximum (FWHM) and θ is the diffraction angle. The average crystallite sizes for as-prepared and 500 °C annealed samples are observed to be 15–18 and 20–32 nm, respectively. The calculated average crystallite size values are listed in Table S1.

The IR spectrum of as-prepared $\text{CaWO}_4:\text{Eu}^{3+}$ (5 at.%)/ Bi^{3+} (1 at.%) sample is shown in Fig. S2. The broad absorption band ranging from 3000–4000 cm^{-1} centered at 3398 cm^{-1} and the band at 1635 cm^{-1} are assigned to O-H stretching and H-O-H bending vibrations. These two bands correspond to the hydrogen-bridging of the water molecules adsorbed on the sample surface which are totally different from the coordinated water complexes [43-45]. The absorption bands at 2943 and 1415 cm^{-1} are assigned as sp^3 C-H stretching and CH_2 bending modes. The $-\text{C}-\text{O}$ and $-\text{COO}^-$ asymmetric stretching modes are assigned to 1455 and 1552 cm^{-1} , respectively [46,47]. The presence of above absorption bands confirms the surface functionalization of PAA. The absorption bands at 834 and 437 cm^{-1} originate from the anti-symmetric stretching vibration and bending vibration in tetrahedral WO_4 group [48-50].

The TEM images obtained for $\text{CaWO}_4:\text{Eu}^{3+}$ (5 at.%)/ Bi^{3+} (5 at.%) sample annealed at 500 °C are displayed in Fig. S3 of the supplementary material. The formation of nanoparticles with irregular shapes and sizes was observed in Fig. S3a. The particle sizes calculated from the TEM image are in the range of 30-40 nm, as shown in the Fig. S3b. The inter-plane spacing calculated from HR-TEM image (Fig. S3c) are found to be 0.33 and 0.19

nm and they correspond to the (112) and (213) planes of the tetragonal CaWO_4 . The selected area electron diffraction (SAED) pattern is shown in Fig. S3d. The indexed diffraction planes correspond to (101), (112), (213), (215) and (402) of tetragonal structure of CaWO_4 .

3.2 Photoluminescence (PL) studies

The photoluminescence excitation (PLE) spectra of the host CaWO_4 sample monitored at different emission wavelengths from 400 to 500 nm (10 nm increment) are shown in Fig. S4a of the supplementary material. The absorption band appeared in the range 230–275 nm is observed in the excitation spectra. This is due to the charge transfer from O^{2-} ligands to the central W^{6+} ions of tetrahedrally coordinated WO_4^{2-} and, this transition is designated as $^1\text{A}_1 \rightarrow ^1\text{T}_1$ which is spin allowed [33]. The emission spectra are observed under the excitation at different wavelengths from 220 to 290 nm (10 nm increment) (Fig. S4b of the supplementary material). The emission band peaking at 420 nm (~350–540 nm) is attributed to $\text{W}^{6+} \rightarrow \text{O}^{2-}$ electronic transition of CaWO_4 and, this is assigned as $^1\text{A}_1 \rightarrow ^3\text{T}_1$ [51]. However, no luminescence has been observed under the excitation of 220, 230, 280 and 290 nm. Meanwhile, the PLE spectra (emission wavelength, $\lambda_{emi} = 400$ to 500 nm with 10 nm increment) of 1 at.% Bi^{3+} doped CaWO_4 nanophosphor are given in Fig. S5a of the supplementary material. All the spectra are composed of two prominent peaks: (i) due to WO_4^{2-} absorption band in the range of 220–278 nm and (ii) a broad band in the range of 279–308 nm centered at 290 nm is assigned to be the $6s^2 \rightarrow 6s6p$ electronic transition of Bi^{3+} ion. The presence of WO_4^{2-} absorption is obvious as the range of λ_{emi} taken is well within the emission range of WO_4^{2-} (refer Fig. S4b). The emission spectra were recorded under different excitation wavelengths of 10 nm increment from 240 to 290 nm (Fig. S5b of the supplementary material). The emission band observed under the excitation of 240 to 270 nm are only related to WO_4^{2-} emission. While the emission bands recorded under the excitation at 280–300 nm are associated solely with Bi^{3+} due to $^3\text{P}_1 \rightarrow ^1\text{S}_0$ transition. This is in conjunction with the nonappearance of emission under the excitation of 280 and 290 nm in CaWO_4 (refer Fig. S4b of the supplementary material).

The PLE spectra (normalized at 270 nm) of as-prepared samples of $\text{CaWO}_4:\text{Eu}^{3+}$ (5 at.%) / Bi^{3+} ($y = 0, 1, 3, 5, 7, 9, 11, 13$ and 15 at.%) monitored at 615 nm emission wavelength are displayed in Fig. 1a. All the spectra show a broad band in the UV region (230 to 325 nm) peaking at ~270 nm. This band is due to the overlapping of both $\text{O}^{2-} \rightarrow \text{W}^{6+}$ ligand absorption and charge transfer band (CTB) originating from electron transfer from oxygen $2p$ states to

the empty $4f$ states of Eu^{3+} ($\text{O}^{2-} \rightarrow \text{Eu}^{3+}$) [37,52]. This can be ascertained from the broadening of full width at half maximum (FWHM) from 18 nm of CaWO_4 to 37 nm of $\text{CaWO}_4:\text{Eu}^{3+}$ (5 at.%) in the excitation band of 230–325 nm region (See Fig. S6 of the supplementary material). In addition to this peak, we can also observe a peak at ~ 290 nm in the $\text{CaWO}_4:\text{Eu}^{3+}$ (5 at.%)/ Bi^{3+} ($y = 1, 3, 5, 7, 9, 13$ and 15 at.%) samples which is related to the Bi^{3+} absorption (discussed in the previous para). Moreover, the sharp lines in the longer wavelength region are also observed. These peaks are originating from the intra configurational $4f-4f$ transitions of Eu^{3+} ions at 362, 376, 381, 393, 416 and 464 nm corresponding to ${}^7\text{F}_0 \rightarrow {}^5\text{D}_4$, ${}^7\text{F}_0 \rightarrow {}^5\text{G}_2$, ${}^7\text{F}_0 \rightarrow {}^5\text{G}_3$, ${}^7\text{F}_0 \rightarrow {}^5\text{L}_6$, ${}^7\text{F}_0 \rightarrow {}^5\text{D}_3$ and ${}^7\text{F}_0 \rightarrow {}^5\text{D}_2$ transitions, respectively. Similarly, same features of excitation can be observed in the 500 °C annealed samples (Fig. 1b). However, one can clearly observe more pronounced Bi^{3+} absorption peak after annealing as compared to as-prepared samples. This may be the indication of Bi^{3+} occupying the lattice sites in the CaWO_4 more perfectly upon annealing as compared to as-prepared samples. Interestingly, in both the spectra, we can observe the enhancement in the $f-f$ absorption intensities with the sensitization of Bi^{3+} , among which, there is a significant enhancement in the absorption lines corresponding to 393 (${}^7\text{F}_0 \rightarrow {}^5\text{L}_6$) and 464 (${}^7\text{F}_0 \rightarrow {}^5\text{D}_2$) nm. In the case of as-prepared samples, the maximum enhancement is observed in $\text{CaWO}_4:\text{Eu}^{3+}$ (5 at.%)/ Bi^{3+} (11 at.%) with ~ 4.8 and ~ 7 fold increase in ${}^7\text{F}_0 \rightarrow {}^5\text{L}_6$ (393 nm) and ${}^7\text{F}_0 \rightarrow {}^5\text{D}_2$ (464 nm) absorptions, respectively (inset of Fig. 1a). While, upon annealing, this enhancement is found to be more by a factor of ~ 5 for ${}^7\text{F}_0 \rightarrow {}^5\text{L}_6$ and ~ 10 for ${}^7\text{F}_0 \rightarrow {}^5\text{D}_2$ in $\text{CaWO}_4:\text{Eu}^{3+}$ (5 at.%)/ Bi^{3+} (5 at.%), as illustrated in the inset of Fig. 1b. The reasons for such enhancement are related to the distortion of crystal field around the Eu^{3+} due to difference in charge states of Ca^{2+} to Bi^{3+} and/or Eu^{3+} and lack of charge compensation that eventually creates vacancies at Ca^{2+} positions in the quest of maintaining the charge neutrality in the system [35,53].

The PL emission spectra of (a) as-prepared and (b) 500 °C annealed $\text{CaWO}_4:\text{Eu}^{3+}$ (5 at.%)/ Bi^{3+} ($y = 0, 1, 3, 5, 7, 9, 11, 13$ and 15 at.%) samples under the 393 nm excitation are displayed in Fig. 2. In the case of as-prepared samples, the emission intensity of Eu^{3+} increases with the increase of Bi^{3+} concentration. The maximum increase is found at $\sim 9-11$ at.% of Bi^{3+} thereafter, it decreases. On the other hand, this emission increase for annealed samples rises up to ~ 5 at.% of Bi^{3+} and, then, it decreases with the further increase of Bi^{3+} concentration. The emission intensity decreases with further increase of Bi^{3+} concentration beyond the mentioned concentration i.e. 11 and 5 at.%, respectively, for as-prepared and annealed samples is understandable, as the Bi^{3+} concentration increases, there is a chance of

clustering among the Bi^{3+} ions leading to the quenching of luminescence. Similar behavior in CaMoO_4 has been reported earlier by us [35]. The identical pattern of emission spectra in both the sets of samples i.e. (a) as-prepared and (b) 500 °C annealed are also observed under the excitation of 464 nm (Fig. 3). The emission bands observed in all the spectra of both figures are related to f - f transitions of Eu^{3+} [54-56]. The emission peaks at 591 nm (${}^5\text{D}_0 \rightarrow {}^7\text{F}_1$) and 655 nm (${}^5\text{D}_0 \rightarrow {}^7\text{F}_3$) are related to parity allowed magnetic dipole transitions. While the strongest peak at 615 nm (${}^5\text{D}_0 \rightarrow {}^7\text{F}_2$) is due to hypersensitive electric dipole transition whereas peak at 702 nm (${}^5\text{D}_0 \rightarrow {}^7\text{F}_4$) is originated from electric quadrupole transitions. In all the spectra shown in both the figures, the electric dipole transition (615 nm) is the strongest among all other observed transitions. Such dominant peak compared to remaining peaks is well explained on the basis of symmetry around the Eu^{3+} environment. In CaWO_4 , the Ca^{2+} sites are coordinated with 8 (eight) oxygen atoms with S_4 point symmetry without inversion center. This leads to the hypersensitive electric dipole transitions of Eu^{3+} whenever Eu^{3+} replaces Ca^{2+} ions in the CaWO_4 crystal. As reported in the previous studies [35,52,57], the possibility of Eu^{3+} and/or Bi^{3+} substitution in the Ca^{2+} lattice sites for charge compensation is as (i) $3\text{Ca}^{2+} \rightarrow 2\text{Eu}^{3+} + \text{Ca}^{2+}$ vacancy and/or (ii) $3\text{Ca}^{2+} \rightarrow 2\text{Bi}^{3+} + \text{Ca}^{2+}$ vacancy. The creation of such vacancies during the crystal formation while doping Eu^{3+} and/or Bi^{3+} also likely to add more asymmetric environment around the Eu^{3+} leading to hypersensitive electric dipole transitions.

As compared to unsensitized $\text{CaWO}_4:\text{Eu}^{3+}$ (5 at.%) in the case of as-prepared samples, the luminescence intensity is substantially increased when $\text{CaWO}_4:\text{Eu}^{3+}$ (5 at.%) is sensitized with 11 at.% of Bi^{3+} . The enhancement is approximately by a factor of ~ 3.5 and ~ 4.5 under the excitation at 393 and 464 nm respectively (Figs. 4a and 4b). While, in the case of 500 °C annealed samples, the enhancement is found to be higher as compared to as-prepared samples with the factor of ~ 5.8 and ~ 22 under the excitation at 393 and 464 nm respectively, when 5 at.% Bi^{3+} is used in $\text{CaWO}_4:\text{Eu}^{3+}$ (5 at.%) (Figs. 4c and 4d). This enhancement in emission was expected. This agrees with the enhanced absorption intensities of the 393 and 464 nm transitions observed in the excitation spectra (Fig. 1). It is worth to mention that the strictly forbidden ${}^5\text{D}_0 \rightarrow {}^7\text{F}_0$ transition at 579 nm, with the note that this transition is allowed in C_s , C_n and C_{nv} site symmetries, is more pronounced in all the Bi^{3+} sensitized emission spectra, as compared to unsensitized samples (insets of Fig. 4). This further corroborates the (i) occupation of Eu^{3+} ions in single equivalent site in the absence of inversion symmetry with more distorted lattice [52,57,58] (ii) indication of more asymmetric

environment due to Bi^{3+} sensitization leading to more enhanced luminescence intensity in both excitation and emission. In Fig. 5, the photographic evidence is shown for red color emission under the exposure to different light sources of 268, 290, 393 and 464 nm of as-prepared $\text{CaWO}_4:\text{Eu}^{3+}$ (5 at.%)/ Bi^{3+} (11 at.%) and 500 °C annealed $\text{CaWO}_4:\text{Eu}^{3+}$ (5 at.%)/ Bi^{3+} (5 at.%) samples.

3.3 Mechanism of energy transfer from Bi^{3+} to Eu^{3+}

To investigate the energy transfer mechanism, we have selected the energy transfer from Bi^{3+} over the $\text{O}^{2-} \rightarrow \text{W}^{6+}$ and/or $\text{O}^{2-} \rightarrow \text{Eu}^{3+}$ to excited states of Eu^{3+} simply because of two reasons: (i) more intense absorption of Bi^{3+} over the other excitation spectra (Fig. 1) in both as-prepared and annealed samples and (ii) not many reports are available on the detail investigation of energy transfer from Bi^{3+} to Eu^{3+} ions in CaWO_4 . For this, a series of samples were prepared with different Eu^{3+} concentrations and fixed Bi^{3+} concentration (say 11 at%). The excitation wavelength was used at 290 nm for all the cases. This wavelength is related to Bi^{3+} absorption and its subsequent emission, as discussed earlier (Fig. S4 and S5 in the supplementary material). The PL (normalized at 590 nm) emission spectra of as-prepared and 500 °C annealed $\text{CaWO}_4:\text{Eu}^{3+}$ ($x = 0, 1, 3, 5, 7, 9, 11, 13$ and 15 at.%)/ Bi^{3+} (11 at.%) under the 290 nm excitation are shown in Figs. 6 and 7, respectively. The inset of the graph shows the enlarged Gaussian fitted broad emission band over 325–565 nm. From the spectra, it is clearly observed that the emission intensity related to Bi^{3+} gradually decreases with the increase of Eu^{3+} concentration. This may be understood as the increase of non-radiative energy transfer from the Bi^{3+} to the excited states of Eu^{3+} ions randomly distributed in the crystal lattice. Such energy transfer is possible because of the overlapping of emission band of Bi^{3+} with the excitation bands of Eu^{3+} (Fig. S7 in the supplementary material). This type of energy transfer is commonly referred as resonance energy transfer. To quantify the extent of energy transfer with the increase of Eu^{3+} concentration, the energy transfer efficiency (η_T) from the sensitizer Bi^{3+} to the activator Eu^{3+} was calculated by using following formula: [30]

$$\eta_T = 1 - \frac{I_s}{I_{s_0}} \quad (2)$$

where η_T is the energy transfer efficiency, I_s and I_{s_0} are the emission intensities of the sensitizer Bi^{3+} in the presence and absence of the activator (i.e. Eu^{3+} in the present case), respectively. The energy transfer efficiency of the as-prepared and 500 °C annealed samples is shown in Fig. 8. The energy transfer efficiency (η_T) for both as-prepared and 500 °C

annealed samples gradually increases with increasing Eu^{3+} concentration with the maximum energy transfer efficiency reaching up to 75% and 95%, respectively.

Typically, a resonance type of energy transfer mechanism can be of two types: (i) exchange interaction and (ii) multipolar interaction. Both the interactions are fully dependent on the distance between the sensitizer and activator ions. The critical distance, R_c for the energy transfer from Bi^{3+} to Eu^{3+} can be calculated by the following formula suggested by Blasse, [59]

$$R_c = 2 \left[\frac{3V}{4\pi x_c N} \right]^{1/3} \quad (3)$$

where, R_c is the critical distance, V is the volume of the unit cell, x_c is the critical concentration and N is the number of host cations in the unit cell. Here, for CaWO_4 host, V is 312.63 \AA^3 , $N = 4$. The critical concentrations are $x_c = 0.2$ and 0.22 , respectively, for annealed and as-prepared samples. Therefore, the critical distance R_c value for the energy transfer of $\text{CaWO}_4:\text{Eu}^{3+}$ (x at.%) / Bi^{3+} (11 at.%) was determined to be $\sim 9 \text{ \AA}$. It is well known that the critical distance for energy transfer by exchange interaction is restricted by 5 \AA . Here, the calculated R_c value exceeds the range of exchange interaction mechanism. Thus, the energy transfer between the Bi^{3+} and Eu^{3+} ions can be considered mainly due to the multipolar interactions. Such multipolar interactions can be identified on the basis of Dexter's energy transfer equation and Reisfeld's approximation, [60]

$$\frac{I_{s_0}}{I_s} \propto C_{\text{Bi}^{3+}+\text{Eu}^{3+}}^{n/3} \quad (4)$$

where C is the total concentration of Bi^{3+} and Eu^{3+} ions in the sample and $n = 6, 8$ and 10 corresponding to dipole-dipole, dipole-quadrupole and quadrupole-quadrupole interactions. The plots between I_{s_0}/I_s and $C_{\text{Bi}^{3+}+\text{Eu}^{3+}}^{n/3}$ for different n values are depicted in Fig. 9 for as-prepared (a-c) and $500 \text{ }^\circ\text{C}$ (d-f) annealed samples. Among different values of n , the best fit of linear plot is observed at $n = 6$ in both the cases with a goodness of $R^2 = 0.9403$ and 0.9753 , respectively. This indicates that the energy transfer from Bi^{3+} to Eu^{3+} in CaWO_4 is mainly through dipole-dipole interactions.

3.4 Decay lifetime and quantum yield study

The luminescence decay lifetime is an important parameter to understand the mechanism of luminescence in phosphors. The photoluminescence decay of $^5\text{D}_0$ level of Eu^{3+}

(615 nm emission) of as-prepared samples of $\text{CaWO}_4:\text{Eu}^{3+}$ sensitized with various Bi^{3+} concentrations are shown in Figs. 10a and 10c, while for 500 °C annealed samples are given in Figs. 10b and 10d. In all the cases, the excitation wavelengths were 393 and 464 nm. All the luminescence decay can be well fitted by mono exponential function given below,

$$I = I_0 \exp\left(-\frac{t}{\tau}\right) \quad (5)$$

where, I is the luminescence intensity at time t , I_0 is the initial luminescence intensity at time $t = 0$ and τ is the luminescence decay lifetime. This suggests the location of Eu^{3+} ions in uniform cation sites, as mentioned in the previous subsection of steady state luminescence. This behavior is also expected as excitation is direct. The typical linear fitting in the logarithmic scale of PL decay profile is presented in Fig. S8 of the supplementary material. The PL decay lifetime values of $^5\text{D}_0$ level of Eu^{3+} in Bi^{3+} sensitized $\text{CaWO}_4:\text{Eu}^{3+}$ as-prepared and 500 °C annealed samples are summarized in Table S2 of the supplementary material. The PL decay lifetime draws two understandings: (i) the lifetime increases with the Bi^{3+} sensitization may be ascertained to the reduction in the non-radiative relaxation of $^5\text{D}_0$ level to the ground states. This may be induced by relaxing the forbidden transitions due to higher distortion of crystal lattice upon addition of Bi^{3+} and (ii) the lifetime increase after annealing the samples when compared to as-prepared samples may be attributed to the removal of non-radiative pathways by various organic groups of capping agent present on the particle surface. On the other hand, the annealing also leads to larger particle size with the formation of more perfect crystals.

3.5 Quantum yield and CIE chromaticity

The quantum yield (φ) is given by the ratio of number of emitted photons to number of photons absorbed by the fluorophore. Generally, it is defined by the measure of ratio of total radiative transition rate (k_r) to the total radiative (k_r) and non-radiative (k_{nr}) transition rates as: [51]

$$\varphi = \frac{k_r}{k_r + k_{nr}} \quad (6)$$

However, experimentally the ' φ ' is calculated as absolute measure using integrating sphere (mentioned in the characterization section) with the following relation,

$$\varphi = \frac{I_{\text{emission}}}{I_{\text{sample holder}} - I_{\text{sample}}} \quad (7)$$

where $I_{emission}$ is the luminescence emission intensity of sample, $I_{sample\ holder}$ is the intensity of light used to excite pure sample holder (Quartz slide mounted on Teflon in the present case), and I_{sample} is the intensity of light used for exciting sample in sample holder. Therefore, difference between areas of $I_{sample\ holder}$ and I_{sample} gives the photons absorbed by the sample. The quantum yield measurements were done for optimized samples i.e. as-prepared, $\text{CaWO}_4:\text{Eu}^{3+}$ (5 at.%) $/\text{Bi}^{3+}$ (11 at.%) and annealed, $\text{CaWO}_4:\text{Eu}^{3+}$ (5 at.%) $/\text{Bi}^{3+}$ (5 at.%) under the excitation wavelengths of 393 and 464 nm. A typical measurement snapshot along with CIE coordinate output of $\text{CaWO}_4:\text{Eu}^{3+}$ (5 at.%) $/\text{Bi}^{3+}$ (5 at.%) under the 464 nm excitation is shown in the supplementary material, Fig. S9. The values measured for as-prepared are 12 and 8%. While for annealed samples, the values are found to be 14 and 17%. The respective excitation wavelengths in both cases are 393 and 464 nm.

The Commission Internationale de l'Éclairage (CIE) chromaticity diagram coordinate calculation allows to predict the color trueness of the light emission theoretically. The calculated CIE coordinates of the as-prepared $\text{CaWO}_4:\text{Eu}^{3+}$ (5 at.%) $/\text{Bi}^{3+}$ ($y = 0, 1, 3, 5, 7, 9, 11, 13$ and 15) samples excited at 393 and 464 nm are listed in Table S3 of the supplementary material. The positions of related points are presented in Fig. S10 of the supplementary material. Similarly, the characteristics of 500 °C annealed $\text{CaWO}_4:\text{Eu}^{3+}$ (5 at.%) $/\text{Bi}^{3+}$ ($y = 0, 1, 3, 5, 7, 9, 11, 13$ and 15) samples excited at 393 and 464 nm are shown in Table S4 and Fig. S11 of the supplementary material. From these results, it can be confirmed that all the samples show the red color emission under these excitation wavelengths. The emitted color from these samples is nearly 100% saturated. A typical calculation for color saturation value for 500 °C annealed $\text{CaWO}_4:\text{Eu}^{3+}$ (5 at.%) $/\text{Bi}^{3+}$ (5 at.%) under the 464 nm excitation is presented in Fig. S12. The calculated color saturation values of as-prepared $\text{CaWO}_4:\text{Eu}^{3+}$ (5 at.%) $/\text{Bi}^{3+}$ (11 at.%) and 500 °C annealed $\text{CaWO}_4:\text{Eu}^{3+}$ (5 at.%) $/\text{Bi}^{3+}$ (5 at.%) under 393 and 464 nm are tabulated in Table S5 of the supplementary material.

Conclusions

The hydrothermally synthesized Bi^{3+} activated $\text{CaWO}_4:\text{Eu}^{3+}$ nanocrystals were thoroughly characterized by XRD, FT-IR and TEM techniques. We have extensively investigated the luminescence properties and energy transfer mechanism of these samples. An enhancement in the intensity of absorption peaks of Eu^{3+} viz ~ 393 nm (${}^7\text{F}_0 \rightarrow {}^5\text{L}_6$) and ~ 464 nm (${}^7\text{F}_0 \rightarrow {}^5\text{D}_2$) is observed upon Bi^{3+} sensitization. The Eu^{3+} emission at 615 nm (${}^5\text{D}_0 \rightarrow {}^7\text{F}_2$) was improved by a factor of ~ 5.8 and ~ 22 under the excitation of 393 and 464 nm,

respectively, when 5 at.% Bi^{3+} was used as sensitizer in $\text{CaWO}_4:\text{Eu}^{3+}$ (5 at.%) after annealing at 500 °C. Reduction in the non-radiative transitions pathways is observed upon annealing the as-prepared samples. A resonance type of energy transfer occurs from Bi^{3+} to the excited states of Eu^{3+} mainly through dipole-dipole interaction. At the optimal concentration of Bi^{3+} , the quantum yield values are found to be (i) 12 and 8% for as-prepared and (ii) 14 and 17% for annealed samples under the excitation at 393 and 464 nm. CIE chromaticity coordinates reveal the nearly 100% saturation of red color emission for optimized samples. These nanophosphors can be promising candidate as red emitter for both n-UV and blue LED pumped w-LEDs for solid state lighting applications.

CRedit authorship contribution statement

Takhe Yaba: Writing – Original Draft, Investigation, Formal analysis. **Ranjoy Wangkhem:** Writing – Review & Editing. **Naorem Shanta Singh:** Supervision, Writing – Original Draft, Writing – Review & Editing.

Acknowledgement

NS Singh thanks the Science & Engineering Research Board (DST), New Delhi, for financial support (CRG Project No. CRG/2018/003154). Takhe Yaba thanks the Ministry of Tribal Affairs, New Delhi for National fellowship for higher education (NFHE) for ST students and Ranjoy Wangkhem thanks the Council of Scientific and Industrial Research (CSIR), New Delhi for Senior Research Fellowship. Authors also thank SAIF, NEHU Shillong and NIT Manipur for TEM and XRD facilities.

Appendix A. Supplementary material

XRD pattern, FTIR spectrum, TEM images, additional PL spectra, Lifetime tabulation, Quantum yield measurement, CIE color coordinates and Color purity calculation.

References

- [1] C.H. Huang, T.M. Chen, A novel single-composition trichromatic white-light $\text{Ca}_3\text{Y}(\text{GaO})_3(\text{BO}_3)_4:\text{Ce}^{3+},\text{Mn}^{2+},\text{Tb}^{3+}$ phosphor for UV-light emitting diodes, *J. Phys. Chem. C* 115 (2011) 2349–2355.
- [2] N. Guo, Y.J. Huang, H.P. You, M. Yang, Y.H. Song, K. Liu, Y.H. Zheng, $\text{Ca}_9\text{Lu}(\text{PO}_4)_7:\text{Eu}^{2+},\text{Mn}^{2+}$: A potential single-phased white-light-emitting phosphor suitable for white-light-emitting diodes, *Inorg. Chem.* 49 (2010) 10907–10913.
- [3] N.S. Singh, R. Wangkhem, T. Yaba, S. Devi, M. N. Luwang, N. Yaiphaba, H. S. Devi, T.D. Singh, Multicolour and nearly white light emission in $\text{YP}_{0.8}\text{V}_{0.2}\text{O}_4:\text{Sm}^{3+}$ nanorods: controlled energy transfer, *J. Alloys Compd.* 726 (2017) 1161–1167.
- [4] C.H. Huang, T.M. Chen, W.R. Liu, Y.C. Chiu, Y.T. Yeh, S. M. Jang, A single-phase emission-tunable phosphor $\text{Ca}_9\text{Y}(\text{PO}_4)_7:\text{Eu}^{2+},\text{Mn}^{2+}$ with efficient energy transfer for white-light-emitting diodes, *ACS Appl. Mater. Interfaces* 2 (2010) 259–264.
- [5] H. Zhou, Y. Jin, M. Jiang, Q. Wang, X. Jiang, A single-phased tunable emission phosphor $\text{MgY}_2\text{Si}_3\text{O}_{10}:\text{Eu}^{3+},\text{Bi}^{3+}$ with efficient energy transfer for white LEDs, *Dalton Trans.* 44 (2015) 1102–1109.
- [6] Z. Xia, Y. Zhang, M.S. Molokeev, V.V. Atuchin, Y. Luo, Linear structural evolution induced tunable photoluminescence in clinopyroxene solid-solution phosphors, *Sci. Reports* 3 (2013) 3310.
- [7] H. Ji, Z. Huang, Z. Xia, M.S. Molokeev, V.V. Atuchin, M. Fang, S. Huang, New yellow-emitting Whitlockite-type structure $\text{Sr}_{1.75}\text{Ca}_{1.25}(\text{PO}_4)_2:\text{Eu}^{2+}$ phosphor for near-UV pumped white light-emitting devices, *Inorg. Chem.* 53 (2014) 5129–5135.
- [8] J. L. Leañó, S-Y. Lin, A. Lazarowska, S. Mahlik, M. Grinberg, C. Liang, W. Zhou, M.S. Molokeev, V.V. Atuchin, Y-T. Tsai, C.C. Lin, H-S. Sheu, R-S. Liu, Green light-excitable Ce-doped nitridomagnesoaluminate $\text{Sr}[\text{Mg}_2\text{Al}_2\text{N}_4]$ phosphor for white light-emitting diodes, *Chem. Mater.* 28(19) (2016) 6822–6825.
- [9] X. Zhang, M. Gong, A new red-emitting $\text{Ce}^{3+},\text{Mn}^{2+}$ -doped barium lithium silicate phosphor for NUV LED application, *Mater. Lett.* 65 (2011) 1756–1758.
- [10] Y. Linghong, Z. Liya, W. Zhengliang, S. Jianhua, G. Fuzhong, W. Weiping, W. Wei, $\text{KGd}(\text{MoO}_4)_2:\text{Eu}^{3+}$ as a promising red phosphor for light-emitting diode application, *Curr. Appl. Phys.* 10 (2010) 208–213.

- [11] S. Nakamura, G. Fasol, *The Blue Laser Diode*, first ed., Springer, Berlin, 1997.
- [12] X. Meng, Y. Wang, Hydrothermal synthesis and luminescent properties of $\text{Li}_x\text{Eu}_x\text{Sr}_{1-2x}\text{MoO}_4$ red phosphor, *J. Rare Earth* 29 (2011) 1040–1044.
- [13] J.K. Park, M.A. Lim, C.H. Kim, H.D. Park, J.T. Park, S.Y. Choi, White light-emitting diodes of GaN-based $\text{Sr}_2\text{SiO}_4 : \text{Eu}$ and the luminescent properties, *Appl. Phys. Lett.* 82 (2003) 683–685.
- [14] V.V. Atuchin, N.F. Beisel, E.N. Galashov, E.M. Mandrik, M.S. Molokeev, A.P. Yelissev, A.A. Yusuf, Z. Xia, Pressure-stimulated synthesis and luminescence properties of microcrystalline $(\text{Lu},\text{Y})_3\text{Al}_5\text{O}_{12}:\text{Ce}^{3+}$ garnet phosphors, *ACS Appl. Mater. Interfaces* 7(47) (2015) 26235–26243.
- [15] H. Ji, L. Wang, M.S. Molokeev, N. Hirosaki, R. Xie, Z. Huang, Z. Xia, O.M. Kate, L. Liu, V.V. Atuchin, Structure evolution and photoluminescence of $\text{Lu}_3(\text{Al},\text{Mg})_2(\text{Al},\text{Si})_3\text{O}_{12}:\text{Ce}^{3+}$ phosphors: new yellow-color converters for blue LED-driven solid state lighting, *J. Mater. Chem. C* 4 (2016) 6855–6863.
- [16] E.N. Galashov, V.V. Atuchin, T.A. Gavriloova, I.V. Korolko, Y.M. Mandri, A.P. Yelissev, Z. Xia, Synthesis of $\text{Y}_3\text{Al}_5\text{O}_{12}:\text{Ce}^{3+}$ phosphor in the $\text{Y}_2\text{O}_3\text{–Al–CeO}_2$ ternary system, *J. Mater. Sci.* 52 (2017) 13033–13039.
- [17] Y. Zhang, W. Gong, J. Yu, Y. Lin, G. Ning, Tunable white-light emission via energy transfer in single-phase $\text{LiGd}(\text{WO}_4)_2:\text{Re}^{3+}$ ($\text{Re}=\text{Tm}, \text{Tb}, \text{Dy}, \text{Eu}$) phosphors for UV-excited WLEDs, *RSC Adv.* 5 (2015) 96272–96280.
- [18] Z.B. Tang, C.L. Xu, X.R. Wei, X.G. Zhang, Y.B. Chen, Improved photoluminescence intensity and thermal stability brought by increasing Eu^{3+} content in $\text{KBaY}_{1-x}\text{Eu}_x\text{Si}_2\text{O}_7$ solid-solution phosphors, *J. Alloys Compd.* 695 (2017) 2745–2750.
- [19] C.F. Guo, J. Yu, X. Ding, M. Li, Z.Y. Ren, J.T. Bai, A dual-emission phosphor $\text{LiCaBO}_3:\text{Ce}^{3+},\text{Mn}^{2+}$ with energy transfer for near-UV LEDs, *J. Electrochem. Soc.* 158 (2011) J42–J46.
- [20] M.M. Shang, G.G. Li, X.J. Kang, D.M. Yang, D.L. Geng, J. Lin, Tunable luminescence and energy transfer properties of $\text{Sr}_3\text{AlO}_4\text{F}:\text{RE}^{3+}$ ($\text{RE} = \text{Tm}/\text{Tb}, \text{Eu}, \text{Ce}$) phosphors, *ACS Appl. Mater. Interfaces* 3 (2011) 2738–2746.
- [21] G. Li, Y. Tian, Y. Zhao, J. Lin, Recent progress in luminescence tuning of Ce^{3+} and Eu^{2+} -activated phosphors for pc-WLEDs, *Chem. Soc. Rev.* 44 (2015) 8688–8713.

- [22] D.Y. Wang, Y.C. Wu, T.M. Chen, Synthesis, crystal structure, and photoluminescence of a novel blue-green emitting phosphor: BaHfSi₃O₉:Eu²⁺ J. Mater. Chem. 21 (2011) 18262–18265.
- [23] R.J. Xie, N. Hirosaki, T. Suehiro, F.F. Xu, M. Mitomo, A simple, efficient synthetic route to Sr₂Si₅N₈:Eu²⁺-based red phosphors for white light-emitting diodes, Chem. Mater. 18 (2006) 5578-5583.
- [24] P. Pust, V. Weiler, C. Hecht, A. Tücks, A.S. Wochnik, A.K. Henß, D. Wiechert, C. Scheu, P.J. Schmidt, W. Schnick, Narrow-band red-emitting Sr[LiAl₃N₄]:Eu²⁺ as a next-generation LED-phosphor material, Nature Mater. 13 (2014) 891-896.
- [25] M. Zeuner, F. Hintze, W. Schnick, Low temperature precursor route for highly efficient spherically shaped LED-phosphors M₂Si₅N₈:Eu²⁺ (M = Eu, Sr, Ba), Chem. Mater. 21 (2009) 336-342.
- [26] S.K. Hussain, J.S. Yu, Broad red-emission of Sr₃Y₂Ge₃O₁₂:Eu²⁺ garnet phosphors under blue excitation for warm WLED applications, RSC Adv. 7 (2017) 13281-13288.
- [27] X. Huang, Red phosphor converts white LEDs, Nat. Photonics (2014) 748-749.
- [28] N.S. Singh, R.S. Ningthoujm, L.R. Devi, N. Yaiphaba, V. Sudarsan, S.D. Singh, R.K. Vatsa, R. Tewari, Luminescence study of Eu³⁺ doped GdVO₄ nanoparticles: Concentration, particle size, and core/shell effects, J. Appl. Phys. 104 (2008) 104307.
- [29] N.S. Singh, R.S. Ningthoujam, M.N. Luwang, S.D. Singh, R.K. Vatsa, Luminescence, lifetime and quantum yield studies of YVO₄:Ln³⁺ (Ln³⁺ = Dy³⁺, Eu³⁺) nanoparticles: Concentration and annealing effects, Chem. Phys. Lett. 480 (2009) 237-242.
- [30] S.H. Lee, Y. Cha, H. Kim, S. Lee, J.S. Yu, Luminescent properties of Eu³⁺-activated Gd₂ZnTiO₆ double perovskite red-emitting phosphors for white light-emitting diodes and field emission displays, RSC Adv. 8 (2018) 11207-11215.
- [31] A.K. Parchur, R.S. Ningthoujam, S.B. Rai, G.S. Okram, R.A. Singh, M. Tyagi, S.C. Gadkari, R. Tewari, R.K. Vasta, Luminescence properties of Eu³⁺ doped CaMoO₄ nanoparticles, Dalton Trans. 40 (2011) 7595-7601.
- [32] W.J. Zhang, W.L. Feng, Y.M. Nie, Photoluminescence properties of red europium doped calcium tungstate phosphors for blue-pumped light-emitting diodes, Optik. 126 (2015) 1341–1343.
- [33] Y. Su, L. Li, G. Li, Synthesis and optimum luminescence of CaWO₄-based red phosphors with codoping of Eu³⁺ and Na⁺, Chem. Mater. 20 (2008) 6060–6067.

- [34] P. Du, J.S. Yu, Eu^{3+} -activated La_2MoO_6 - La_2WO_6 red-emitting phosphors with ultrabroad excitation band for white light-emitting diodes, *Sci. Reports* 7 (2017) 11953.
- [35] R. Wangkhem, T. Yaba, N.S. Singh, R.S. Ningthoujam, Red emission enhancement from $\text{CaMoO}_4:\text{Eu}^{3+}$ by co-doping of Bi^{3+} for near UV/blue LED pumped white pcLEDs: Energy transfer studies, *J. Appl. Phys.* 123 (2018) 124303.
- [36] T. Yaba, R. Wangkhem, N.S. Singh, Photoluminescence properties of Dy^{3+} activated CaWO_4 nanophosphors: a potential single phase near white light emitter, *J. Fluoresce.* 29 (2019) 435-443.
- [37] P. Du, L.K. Bharat, J.S. Yu, Strong red emission in $\text{Eu}^{3+}/\text{Bi}^{3+}$ ions codoped CaWO_4 phosphors for white light-emitting diode and field-emission display applications, *J. Alloys Compd.* 633 (2015) 37–41.
- [38] R.B. Pode, S.J. Dhoble, Photoluminescence in $\text{CaWO}_4:\text{Bi}^{3+},\text{Eu}^{3+}$ material, *Phys. Stat. Sol. (b)* 203 (1997) 571-577.
- [39] B. Liu, L. Peng, Photoluminescent properties of Na^+ , Bi^{3+} co-doped $\text{CaWO}_4:\text{Eu}^{3+}$ phosphor for PDPs, *Appl. Mech. Mater.* 341-342 (2013) 229-232.
- [40] M. Xia, Z. Ju, H. Yang, Z. Wang, X. Gao, F. Pan, X. Liu, Red-emitting enhancement by inducing lower crystal field symmetry of Eu^{3+} site in $\text{CaWO}_4:\text{Eu}^{3+}$ phosphor for n-UV w-LEDs, *J. Alloys Compd.* 739 (2018) 439-446.
- [41] G. Liu, S. Li, Y. Lu, J. Zhang, Z. Feng, C. Li, Controllable synthesis of α - Bi_2O_3 and γ - Bi_2O_3 with high photocatalytic activity by α - $\text{Bi}_2\text{O}_3 \rightarrow \gamma$ - $\text{Bi}_2\text{O}_3 \rightarrow \alpha$ - Bi_2O_3 transformation in a facile precipitation method, *J. Alloys Compd.* 689 (2016) 787-799.
- [42] A.L. Patterson, The scherrer formula for X-ray particle size determination, *Phys Rev.* 56 (1939) 978–982.
- [43] N.N. Golovnev, M.S. Molokeev, S.N. Vereshchagin, V.V. Atuchin, M.Y. Sidorenko, M.S. Dmitrushkov, Crystal structure and properties of the precursor $[\text{Ni}(\text{H}_2\text{O})_6](\text{HTBA})_2 \cdot 2\text{H}_2\text{O}$ and the complexes $\text{M}(\text{HTBA})_2(\text{H}_2\text{O})_2$ ($\text{M} = \text{Ni}, \text{Co}, \text{Fe}$), *Polyhedron* 70 (2014) 71–76.
- [44] N.N. Golovnev, M.S. Molokeev, S.N. Vereshchagin, V.V. Atuchin, Synthesis and thermal transformation of a neodymium(III) complex $[\text{Nd}(\text{HTBA})_2(\text{C}_2\text{H}_3\text{O}_2)(\text{H}_2\text{O})_2] \cdot 2\text{H}_2\text{O}$ to non-centrosymmetric oxosulfate $\text{Nd}_2\text{O}_2\text{SO}_4$, *J. Coord. Chem.* 68(11) (2015) 1865-1877.

- [45] N.N. Golovnev, M.S. Molocheev, A.S. Samoilo, V.V. Atuchin, Influence of alkyl substituents in 1,3-diethyl-2-thiobarbituric acid on the coordination environment in $M(H_2O)_2(1,3\text{-diethyl-2-thiobarbiturate})_2$ $M = Ca^{2+}, Sr^{2+}$, *J. Coord. Chem.* 69(6) (2016) 957-965.
- [46] C.W. Liew, H.M. Ng, A. Numan, S. Ramesh, Poly(acrylic acid)-based hybrid inorganic-organic electrolytes membrane for electrical double layer capacitors application, *Polymers* 8 (2016) 179.
- [47] J.S. Shaikh, R.C. Pawar, N.L. Tarwal, D.S. Patil, P.S. Patil, Supercapacitor behavior of CuO-PAA hybrid films: Effect of PAA concentration, *J. Alloys Compd.* 509 (2011) 7168-7174.
- [48] K.G. Sharma, N.S. Singh, Y.R. Devi, N.R. Singh, S.D. Singh, Effects of annealing on luminescence of $CaWO_4:Eu^{3+}$ nanoparticles and its thermoluminescence study, *J. Alloys Compd.* 556 (2013) 94-101.
- [49] C.S. Lim, A. Aleksandrovsky, M. Molocheev, A. Oreshonkov, V. Atuchin, Microwave sol-gel synthesis and upconversion photoluminescence properties of $CaGd_2(WO_4)_4:Er^{3+}/Yb^{3+}$ phosphors with incommensurately modulated structure, *J. Solid State Chem.* 228 (2015) 160-166.
- [50] C.S. Lim, V.V. Atuchin, A.S. Aleksandrovsky, Y.G. Denisenko, M.S. Molocheev, A.S. Oreshonkov, Fabrication of microcrystalline $NaPbLa(WO_4)_3:Yb^{3+}/Ho^{3+}$ phosphors and their upconversion photoluminescent characteristics, *Korean J. Mater. Res.* 29(12) (2019) 741-746.
- [51] W.M. Yen, S. Shionoya, H. Yamamoto (Eds.), *Phosphor Handbook*, second ed., CRC Press, Taylor & Francis Group, Florida, 2007.
- [52] Y. Su, L. Li, G. Li, Synthesis and optimum luminescence of $CaWO_4$ -Based Red phosphors with codoping of Eu^{3+} and Na^+ , *Chem. Mater.* 20 (2008) 6060-6067.
- [53] S. Yan, J. Zhang, X. Zhang, S. Lu, X. Ren, Z. Nie, X. Wang, Enhanced Red Emission in $CaMoO_4:Bi^{3+}, Eu^{3+}$, *J. Phys. Chem. C* 111 (2007) 13256-13260.
- [54] H. Ji, Z. Huang, Z. Xia, M. S. Molocheev, V.V. Atuchin, M. Fang, Y. Liu, Discovery of new solid solution phosphors via cation substitution-dependent phase transition in $M_3(PO_4)_2:Eu^{2+}$ ($M = Ca/Sr/Ba$) quasi-binary sets, *J. Phys. Chem. C* 119(4) (2015) 2038-2045.

- [55] H. Ji, Z. Huang, Z. Xia, M.S. Molokeev, X. Jiang, Z. Lin and V.V. Atuchin, Comparative investigations of the crystal structure and photoluminescence property of eulytite-type $\text{Ba}_3\text{Eu}(\text{PO}_4)_3$ and $\text{Sr}_3\text{Eu}(\text{PO}_4)_3$, *Dalton Trans.* 44(16) (2015) 7679-7686.
- [56] V.V. Atuchin, A.K. Subanakov, A.S. Aleksandrovsky, B.G. Bazarov, J.G. Bazarova, T.A. Gavrilova, A.S. Krylov, M.S. Molokeev, A.S. Oreshonkov, S.Yu. Stefanovich, Structural and spectroscopic properties of new noncentrosymmetric self-activated borate $\text{Rb}_3\text{EuB}_6\text{O}_{12}$ with B_5O_{10} units, *Mater. Des.* 140 (2018) 488-494.
- [57] W. Wang, P. Yang, Z. Cheng, Z. Hou, C. Li, J. Lin, Patterning of red, green, and blue luminescent films based on $\text{CaWO}_4:\text{Eu}^{3+}$, $\text{CaWO}_4:\text{Tb}^{3+}$, and CaWO_4 phosphors via microcontact printing route, *ACS Appl. Mater. Interfaces* 3 (2011) 3921–3928.
- [58] Y. Huang, H. Lin, H.J. Seo, Luminescence properties and local structures of Eu^{3+} in $\text{EuBaB}_9\text{O}_{16}$ crystal, *J. Electrochem. Soc.* 157(12) (2010) J405-J409.
- [59] G. Blasse, Energy transfer in oxidic phosphors, *Phys. Lett. A* 28 (1968) 444–445.
- [60] D.L. Dexter, A theory of sensitized luminescence in solids, *J. Chem. Phys.* 21 (1953) 836–850.

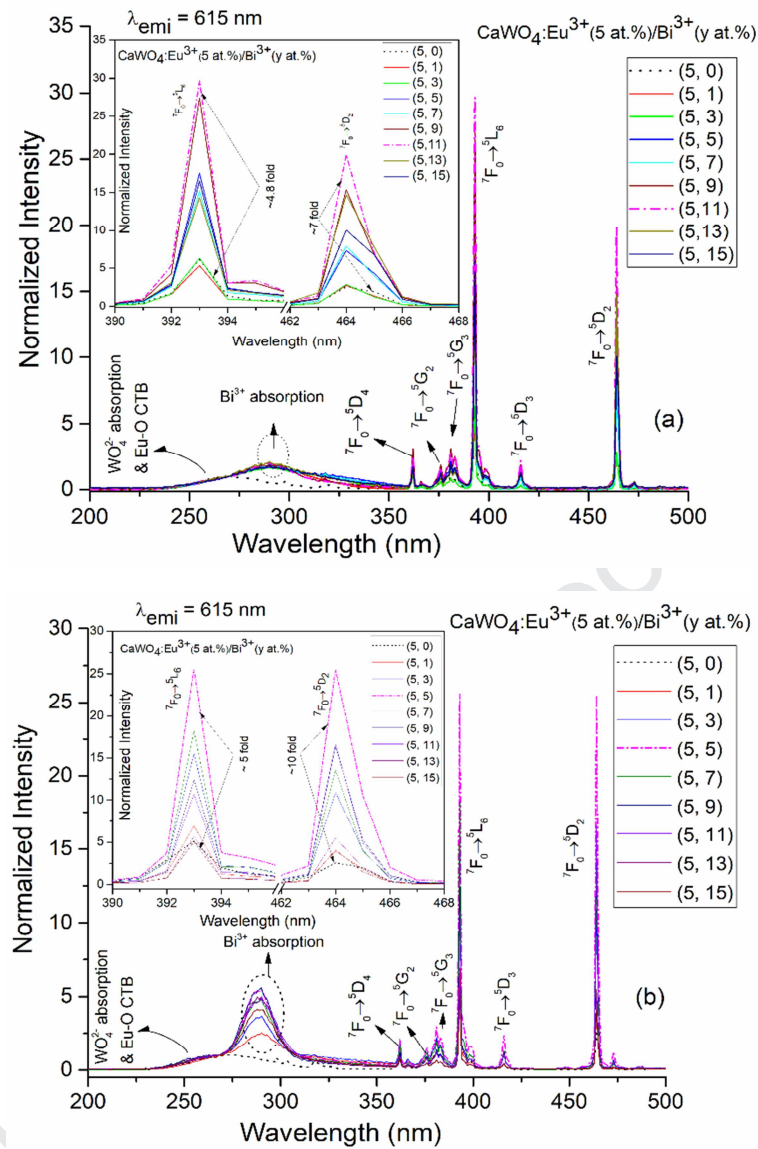


Fig. 1. Excitation spectra of (a) as-prepared and (b) 500 °C annealed $\text{CaWO}_4:\text{Eu}^{3+}$ (5 at.%) / Bi^{3+} ($y = 0, 1, 3, 5, 7, 9, 11, 13$ and 15 at.%) samples monitored at 615 nm emission wavelength.

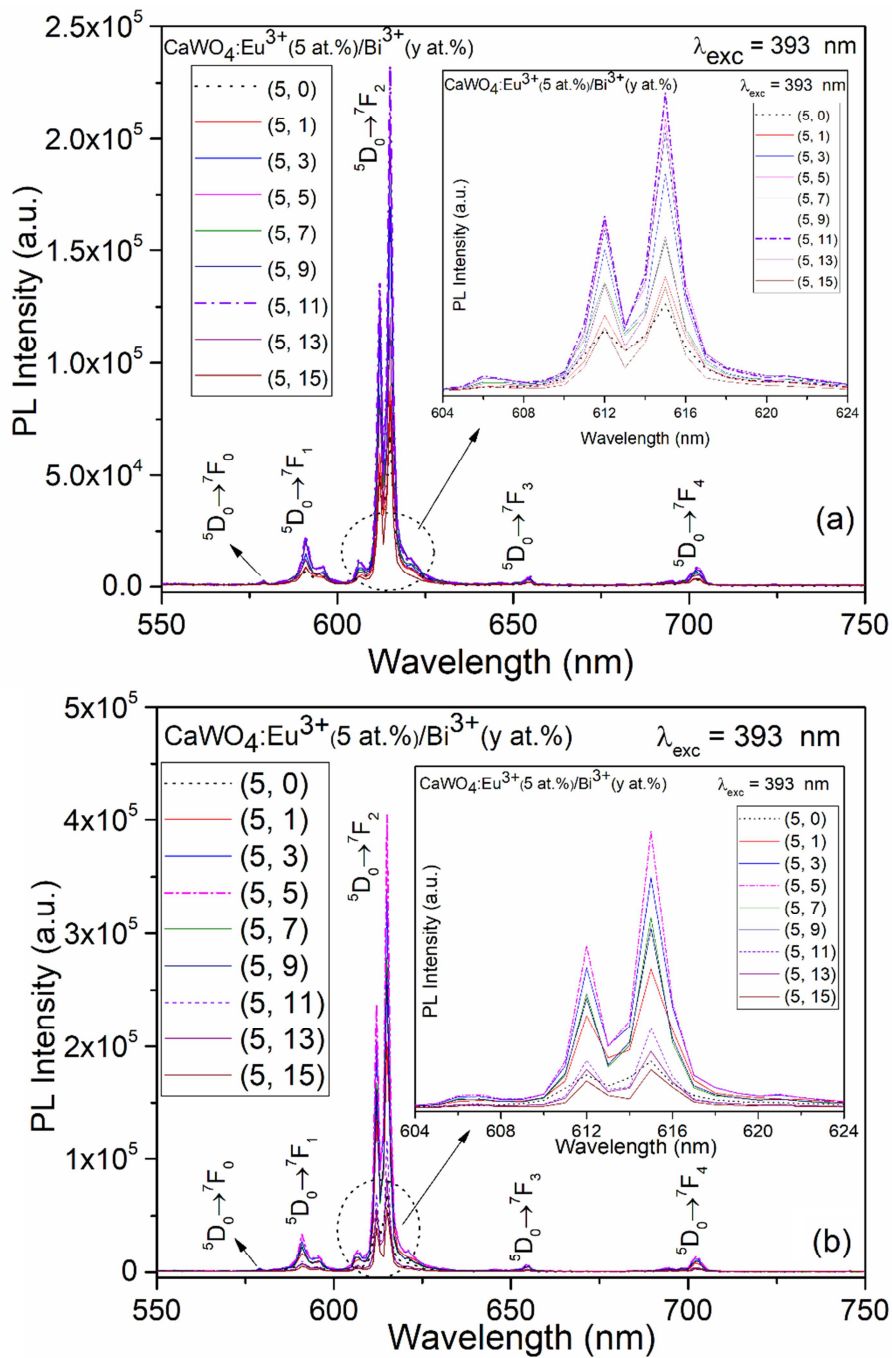


Fig. 2. Emission spectra of (a) as-prepared and (b) 500 °C annealed $\text{CaWO}_4:\text{Eu}^{3+}(5 \text{ at.})/\text{Bi}^{3+}(y \text{ at.})$ ($y = 0, 1, 3, 5, 7, 9, 11, 13$ and 15 at.%) samples under 393 nm excitation.

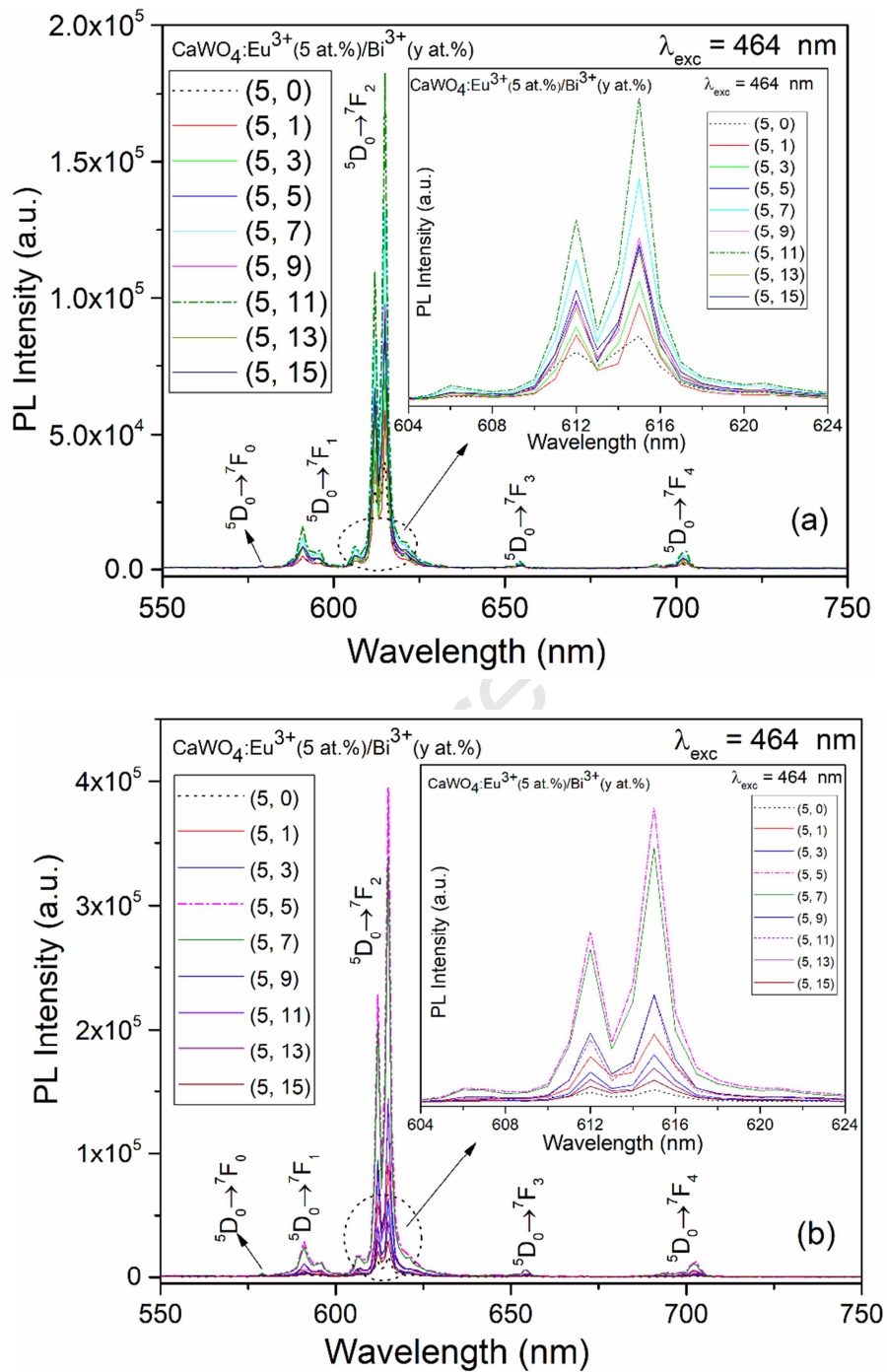


Fig. 3. Emission spectra of (a) as-prepared and (b) 500 °C annealed $\text{CaWO}_4:\text{Eu}^{3+}(5 \text{ at.})/\text{Bi}^{3+}(y \text{ at.})$ samples under 464 nm excitation.

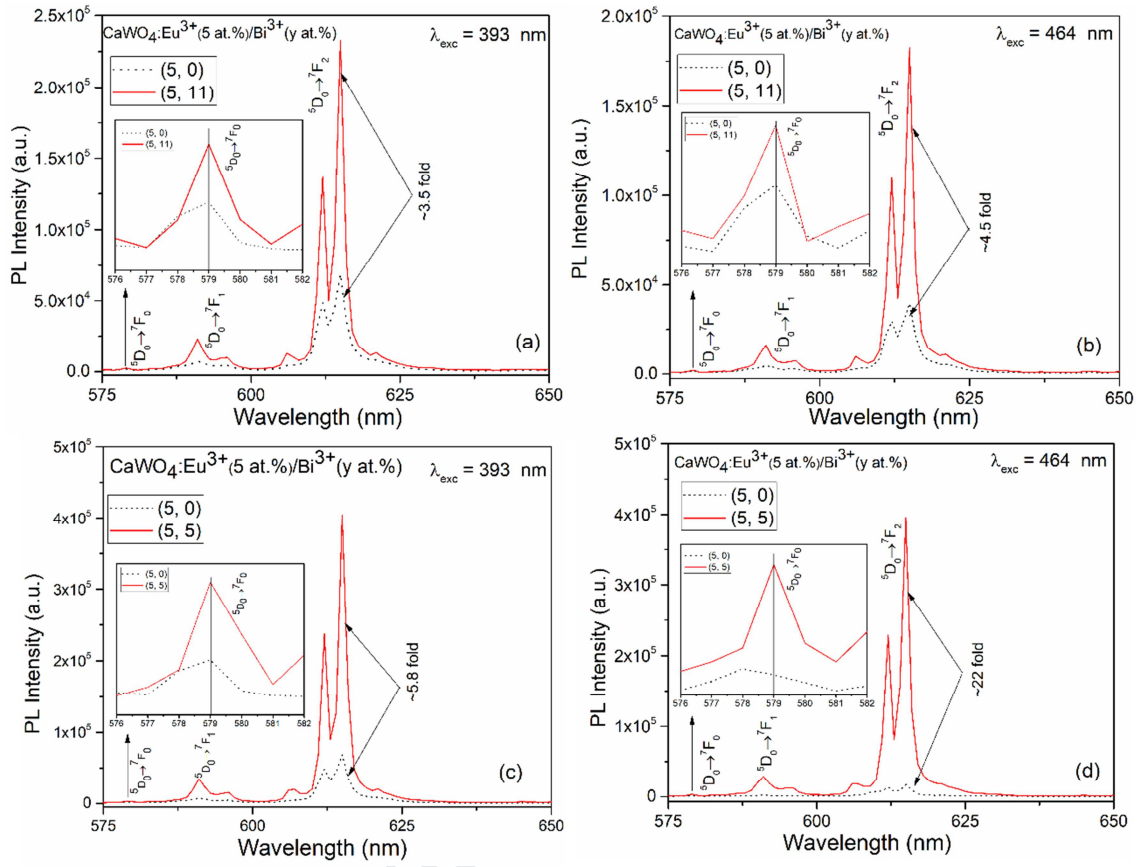


Fig. 4. Comparison of PL emission intensities of (a and b) as-prepared $\text{CaWO}_4:\text{Eu}^{3+}$ (5 at.%)/ Bi^{3+} ($y = 0$ and 11 at.%) and (c and d) 500 °C annealed $\text{CaWO}_4:\text{Eu}^{3+}$ (5 at.%)/ Bi^{3+} ($y = 0$ and 5 at.%) samples under the 393 and 464 nm excitations.

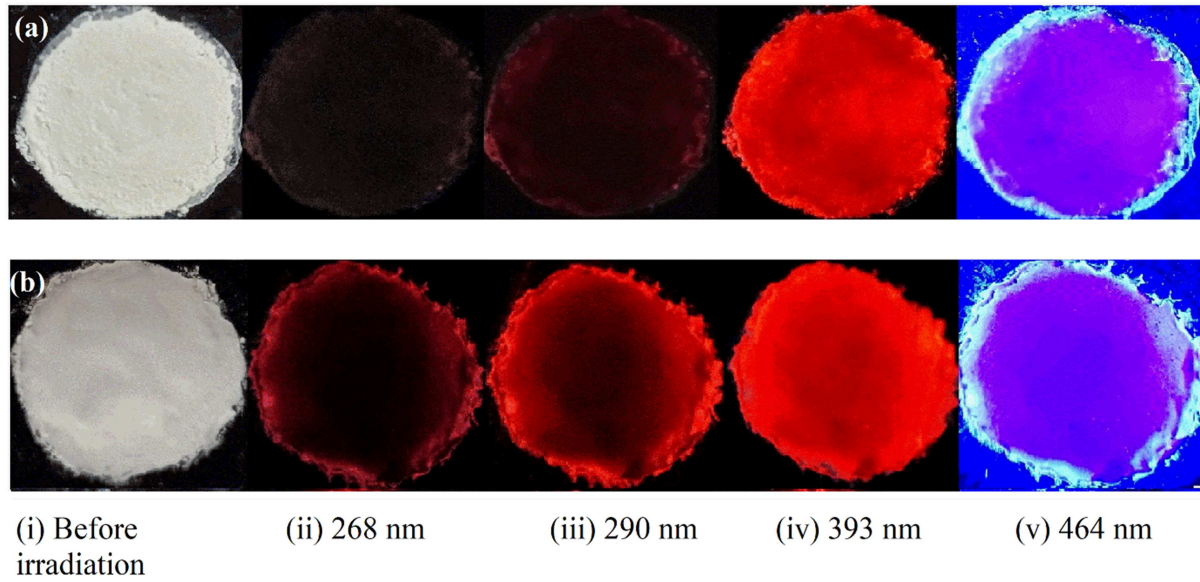


Fig. 5. Photographs of (a) as-prepared $\text{CaWO}_4:\text{Eu}^{3+}$ (5 at.%) / Bi^{3+} (11 at.%) and (b) 500 °C annealed $\text{CaWO}_4:\text{Eu}^{3+}$ (5 at.%) / Bi^{3+} (5 at.%) sample under the exposure to different light sources of (i) 268, (ii) 290, (iv) 393 and (v) 464 nm.

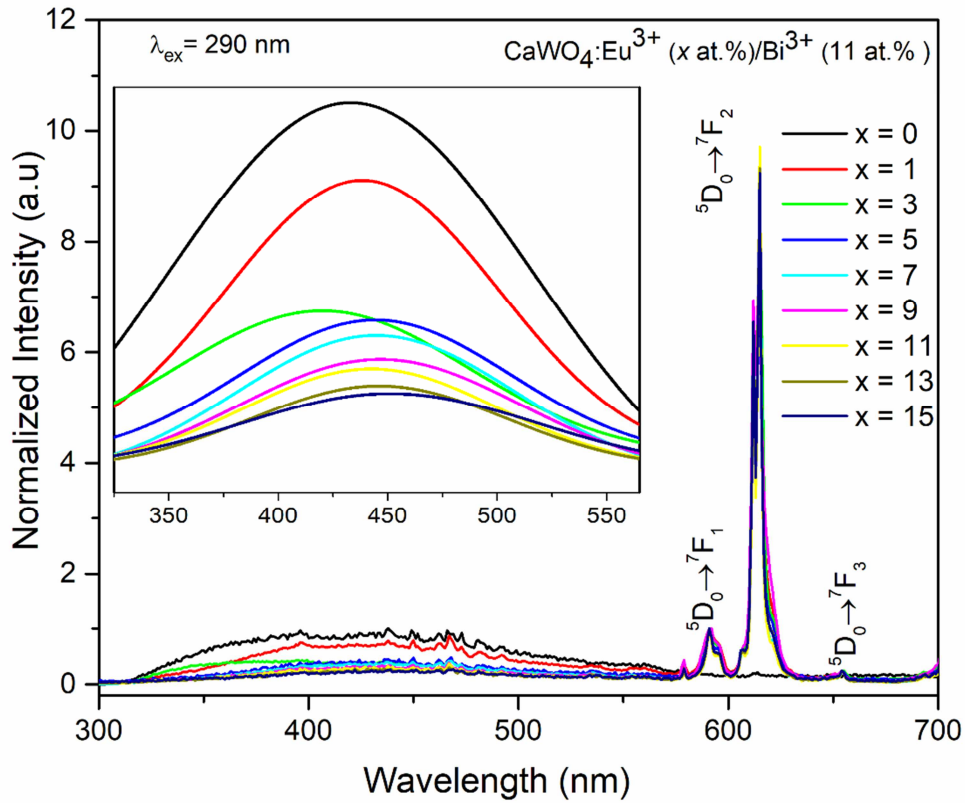


Fig. 6. Normalized (at 590 nm) emission spectra of as-prepared $\text{CaWO}_4:\text{Eu}^{3+}$ ($x = 0, 1, 3, 5, 7, 9, 11, 13$ and 15 at.%) $/\text{Bi}^{3+}$ (11 at.%) under 290 nm excitation. The inset is the enlarged Gaussian fitted broad emission band between 325–565 nm.

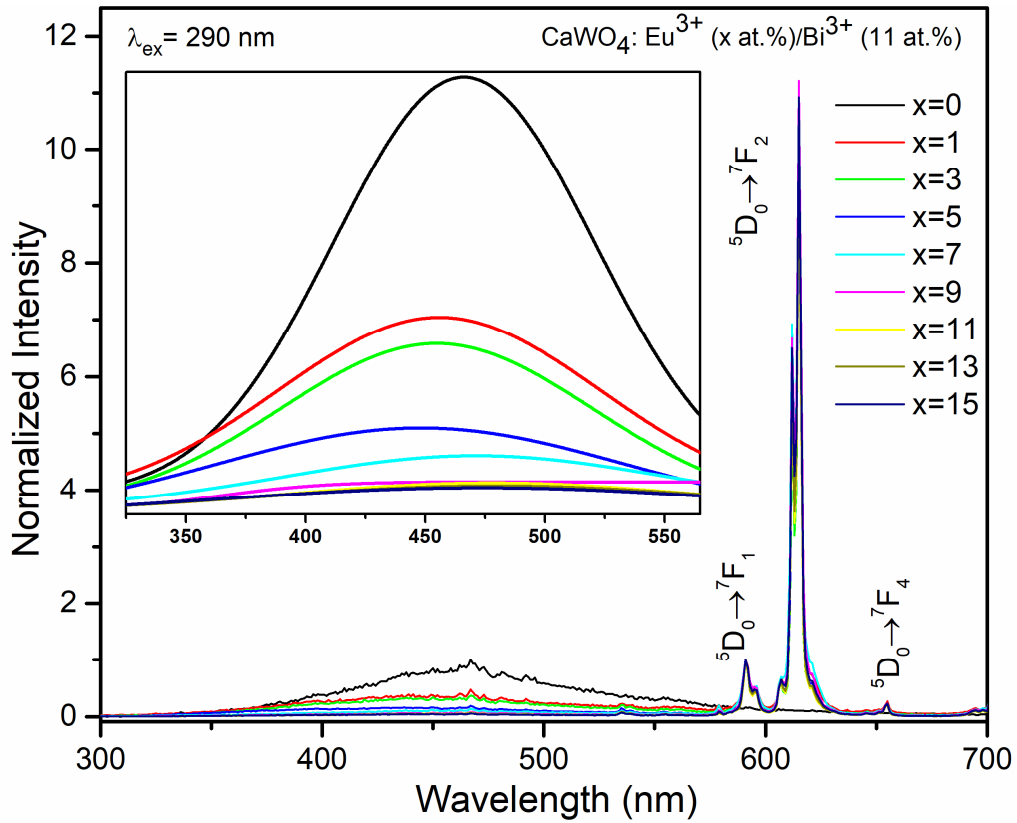


Fig. 7. Normalized (at 590 nm) emission spectra of 500 °C annealed $\text{CaWO}_4:\text{Eu}^{3+}$ ($x = 0, 1, 3, 5, 7, 9, 11, 13$ and 15 at.%) Bi^{3+} (11 at.%) under 290 nm excitation. The inset is the enlarged Gaussian fitted broad emission band between 325–565 nm.

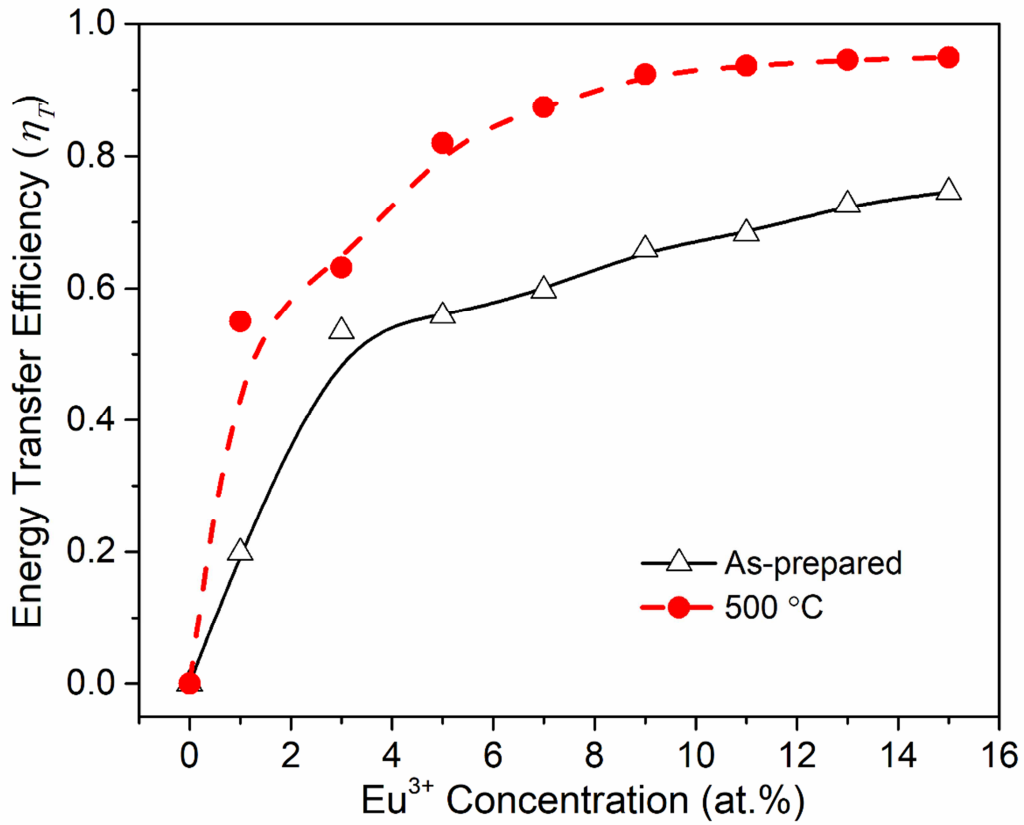


Fig. 8. Energy transfer efficiency (η_T) of different concentration of Eu^{3+} ($x = 0, 1, 3, 5, 7, 9, 11, 13$ and 15 at.%) in Bi^{3+} (11 at.%) sensitized CaWO_4 of as-prepared (black solid line with Δ symbol) and 500°C annealed (red dashed line with \bullet symbol) samples. Excitation wavelength for both cases was 290 nm.

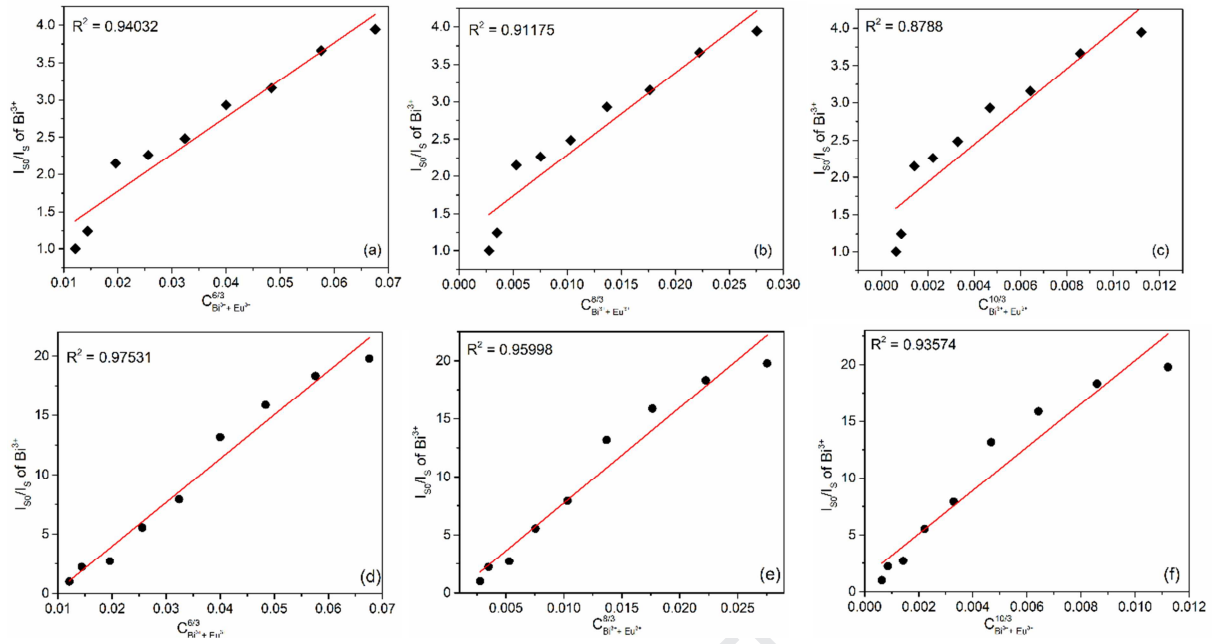


Fig. 9. Dependence of I_{50}/I_S of Bi^{3+} on (a) $C_{\text{Bi}^{3+}+\text{Eu}^{3+}}^{6/3}$, (b) $C_{\text{Bi}^{3+}+\text{Eu}^{3+}}^{8/3}$, (c) $C_{\text{Bi}^{3+}+\text{Eu}^{3+}}^{10/3}$ (as-prepared) and (d) $C_{\text{Bi}^{3+}+\text{Eu}^{3+}}^{6/3}$, (e) $C_{\text{Bi}^{3+}+\text{Eu}^{3+}}^{8/3}$, (f) $C_{\text{Bi}^{3+}+\text{Eu}^{3+}}^{10/3}$ (annealed at 500 °C). Excitation wavelength for both cases was 290 nm.

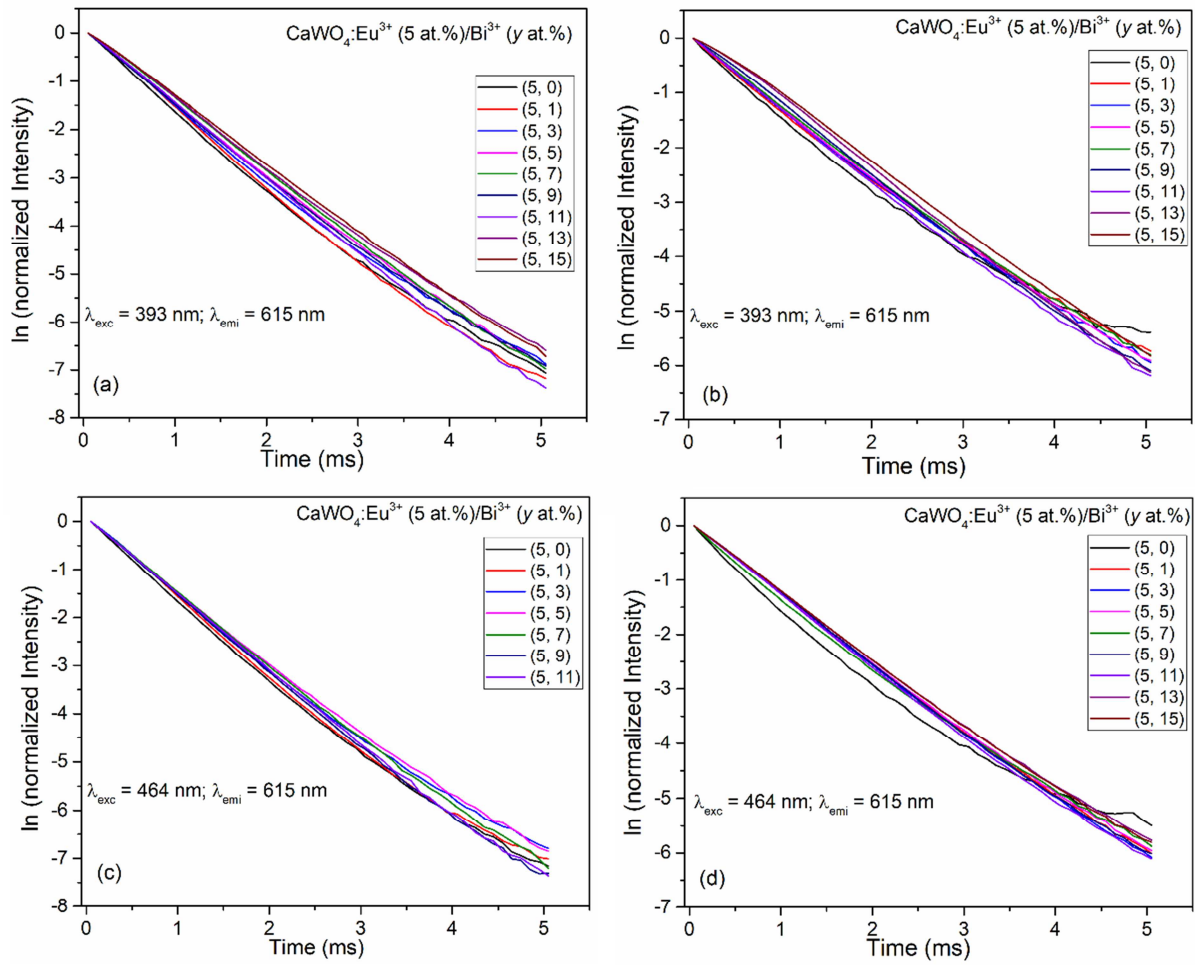


Fig. 10. PL decay profiles of 5D_0 (emission = 615 nm) level of Eu^{3+} in $\text{CaWO}_4:\text{Eu}^{3+}$ (5 at. %)/ Bi^{3+} (y at. %) (a and c) as-prepared un 393 nm and (b and d) 500 °C annealed samples under 464 nm excitation wavelengths.

Highlights

- Red emission enhancement in $\text{CaWO}_4:\text{Eu}^{3+}$ (5 at.%) phosphor with Bi^{3+} sensitization
- All the samples can be excited by near UV (393 nm) and blue (464 nm) light
- Improvement in the energy transfer efficiency from Bi^{3+} to Eu^{3+} upon annealing
- Mode of energy transfer from Bi^{3+} to Eu^{3+} is mainly through dipole-dipole interaction
- Nearly 100% colour saturation in both near UV and blue light excitations are observed

Declaration of interests

The authors declare that they have no known competing financial interests or personal relationships that could have appeared to influence the work reported in this paper.

The authors declare the following financial interests/personal relationships which may be considered as potential competing interests: